

Hybrid improved fuzzy C-means and watershed segmentation to classify Alzheimer's using deep learning

Esraa H. Ali^{1, 2}, Sawsan Sadek¹, Zaid F. Makki³

¹Doctoral School of Sciences and Technology, Lebanese University, Beirut, Lebanon

²Department of Computer Science, College of Science, Al-Nahrain University, Baghdad, Iraq

³Al-Nahrain Center for Strategic Studies, Baghdad, Iraq

Article Info

Article history:

Received Jan 19, 2024

Revised Mar 24, 2024

Accepted Jun 1, 2024

Keywords:

Alzheimer's disease

Convolutional neural network

Improved fuzzy C-means

Magnetic resonance imaging

Watershed segmentation

ABSTRACT

Brain damage and deficits in interactions among brain cells are the primary causes of dementia and Alzheimer's disease (AD). Despite ongoing research, no effective medications have yet been developed for these conditions. Therefore, early detection is crucial for managing the progression of these disorders. In this study, we introduce a novel tool for detecting AD using non-invasive medical tests, such as magnetic resonance imaging (MRI). Our method employs fuzzy C-means clustering to identify features that enhance image accuracy. The standard fuzzy C-means algorithm has been augmented with fuzzy components to improve clustering performance. This enhanced approach optimizes segmentation by extracting image information and utilizing a sliding window to calculate center coordinates and establish a stable group matrix. These critical features are subsequently integrated with a two-phase watershed segmentation process. The resulting segmented images are then used to train an optimal convolutional neural network (CNN) for AD classification. Our methodology demonstrated a 98.20% accuracy rate in the detection and classification of segmented MRI brain images, highlighting its efficacy in identifying disease types.

This is an open access article under the [CC BY-SA](#) license.



Corresponding Author:

Esraa H. Ali

Doctoral School of Sciences and Technology, Lebanese University

Al-Hadath District, Beirut, Lebanon

Email: esraa.ali@ul.edu.lb

1. INTRODUCTION

Alzheimer's disease (AD) is the leading cause of dementia among older adults, characterized as a mental health disorder that results in brain damage and impairs the ability to perform daily activities [1]. It is a chronic neurodegenerative condition with an insidious onset and gradually worsening symptoms over time. The etiology of AD remains unclear, and treatments are often expensive. In recent years, there has been a significant focus on early d AD is the leading cause of dementia among older adults, characterized as a mental health disorder that results in brain damage and impairs the ability to perform daily activities. It is a chronic neurodegenerative condition with an insidious onset and gradually worsening symptoms over time. The etiology of AD remains unclear, and treatments are often expensive. In recent years, there has been a significant focus on early detection of this form of dementia by academics and researchers. The current global demographic of individuals with dementia is estimated to be 47.5 million, projected to increase to 75 million by 2030 [2], [3]. The advancement of digital neuroimaging techniques has enhanced the analysis of clinical imaging data for diagnosing brain disorders. Techniques such as magnetic resonance imaging (MRI), cerebrospinal fluid (CSF) analysis, single photon emission computed tomography (SPECT), and fluorodeoxyglucose positron emission tomography (FDG-PET) are instrumental in identifying structural

changes in the brain. Since the early 1980s, the medical community has begun utilizing these advanced medical imaging techniques to improve the quality of healthcare imagery [4], [5]. The evolution of traditional image processing methods alongside machine learning (ML) and deep learning (DL) has led to significant advancements in medical image analysis. Analytical image processing techniques are categorized into registration, classification, detection, segmentation, and localization, with segmentation being a crucial step in isolating the desired tissue or region of interest (RoI) from the collected images [6], [7].

The model architecture for diagnosing AD encompasses five key stages: data acquisition, segmentation, registration, morphometry, and classification. Various standard datasets, such as Alzheimer's disease neuroimaging initiative (ADNI), international consortium for brain mapping (ICBM), minimal interval resonance imaging in Alzheimer's disease (MIRIAD), Kaggle, open access series of imaging studies (OASIS), Harvard Medical School, and others, are utilized to gather extensive data from morphological and anatomical images. These images are essential for identifying abnormalities in the affected brain. Effective segmentation and classification, particularly in MRI studies, necessitate a robust image pre-processing approach. In the development of Alzheimer's detection systems, processes such as noise reduction, smoothing, skull stripping, cropping, and normalization are indispensable. Through the registration process, images are aligned to a standard reference area, facilitating intra-image and inter-image matching crucial for tracking disease progression and identifying affected individuals [8]. Classification, the final stage, involves categorizing patients as normal or exhibiting abnormalities. Artificial intelligence (AI), in conjunction with MRI, emerges as a promising method for disease classification. The development and application of ML and DL are pivotal in crafting AI-based classification algorithms that enhance outcomes, quality, and efficiency [9].

In various studies, convolutional neural network (CNN)-based learning has been found to lack robustness, prompting the exploration of alternative methods to enhance performance. For MRI brain images, a hybrid approach combining enhanced fuzzy C-means clustering with watershed segmentation (Ws) has been utilized as a feature detection and extraction mechanism to delineate gray matter (GM), white matter (WM), and CSF regions of the brain. Our literature review revealed that limited research has been conducted on developing specialized CNN architectures for more effective AD.

The technique proposed in [10] initiates with a genetic algorithm (GA) for feature selection, identifying the most informative subset of features. Fuzzy C-means (FCM) clustering is applied to this selected subset. This approach reduces the dimensionality of the feature space, thereby rendering the classification process via support vector machine (SVM) both more efficient and understandable. It notably enhances the accuracy of early AD detection by accentuating the differentiation between AD and non-AD clusters. The results underscore the efficacy of this technique in precisely identifying individuals at risk of Alzheimer's at an early stage. To track AD progression, Sappagh *et al.* [11] introduced a multi-modal ensemble DL technique that extracted both local and longitudinal information from each modality. Additionally, prior knowledge was utilized to derive local features from MRI, positron emission tomography (PET), cognitive scores, neuropathology, and ADNI assessments. Employing a combination of layered CNN-bidirectional long short-term memory (BiLSTM), all gathered features were integrated for regression and classification tasks. A multi-modal approach for automated hippocampus segmentation using 3D patches was detailed [12]. Utilizing sMRI (T1) images from the ADNI dataset, a hybrid multi-task deep CNN and 3D DenseNet+softmax were employed for AD classification. The model achieved an accuracy of 88%, sensitivity 86%, and an area under the curve (AUC) of 92% [13]. This study presents a method for early detection of Alzheimer's using SVMs trained on various texture descriptors, which aid in dimensionality reduction derived from MRI alongside SVMs trained on markers obtained from ADNI. Different feature selection methods, each training a distinct SVM, were applied to reduce the dimensionality of voxel-based features. Geetha and Pugazhenthii [14] suggests a novel approach for Alzheimer's classification from MRIs using a fuzzy neural network (FNN). The wavelet transformation (WT) is employed for image decomposition, with the discrete wavelet transform calculating the output coefficient vectors. These generated features are then used to train FNN. A CNN model is proposed for AD classification using MR images with hippocampus designated as the RoI [15]. The RoI is extracted through an automated patch-based separation method that utilizes geometric values from the international consortium for brain mapping (ICBM) standard. CNN was applied for dataset classification, demonstrating notable performances. A novel methodology combining extreme learning and deep learning for AD classification is introduced [16]. This approach evaluates two deep learning models for functional brain-network classification, alongside an extreme learning machine (ELM) enhanced framework for learning deep regional-connectivity and deep adjacent positional features. The construction of the brain network utilizes the Pearson correlation coefficient. In summary, our review highlights three key findings:

- The majority of the literature were reviewed reported evaluation scores below 92%, whereas our study achieved an exceptional performance of 98%. This significant advancement is attributed to our novel segmentation and feature extraction model, which effectively reduces variable parameters while enhancing computational speed.

- Our research introduces a potent classification architecture that utilize different kernel sizes to extract essential features. By incorporating two smaller kernels (3×3 and 5×5), our model achieves robust training and testing processes, thereby improving its performance and reliability.
- Furthermore, our study leverages a substantial dataset comprising 6400 brain images, categorized into four distinct classes: mild, normal, moderate, and very mild. This extensive dataset offers a comprehensive view across various stages of AD, thereby enriching the depth and diversity of our analysis.

2. METHOD

In this paper, we utilize the improved fuzzy C-means clustering (ImFCm) for segmenting brain tissue, owing to its efficiency in segmenting homogeneous intensity regions of MRI images. We introduce a hybrid approach combining ImFCm with Ws, achieving more effective results in accurately partitioning images and enhancing classification performance. The outcomes of these two methods are then integrated into an optimized CNN architecture, aiming to improve the accuracy and robustness of the AD detection system. The ADNI dataset was employed to validate the findings, with approximately 6400 MRI brain images analyzed. These images are annotated into four categories: mild, moderate, very mild, and normal. Figure 1 illustrates the block diagram of the proposed approach. Each section of our method is explained in detail in the subsequent sections.

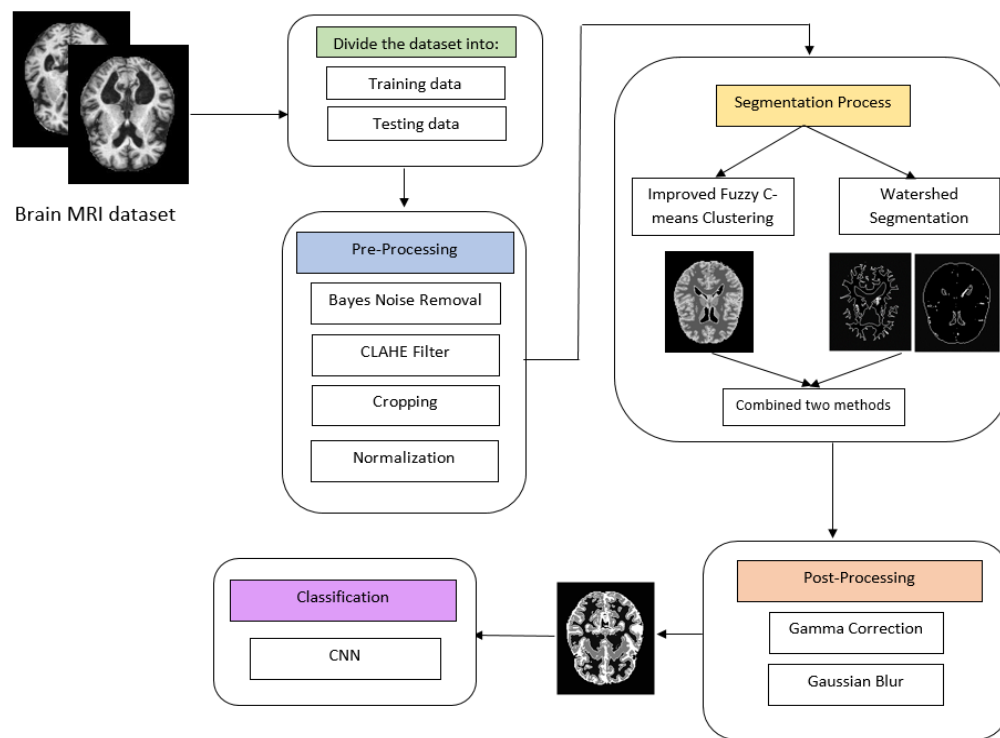


Figure 1. The proposed method

2.1. Pre-processing

Preprocessing is a technique of image enhancement that focus on both the data structure and processing constraints. It encompasses the removal enhancement of the image to improve system performance. Cropping is used to eliminate unnecessary components from an image. Additionally, converting the images to grayscale, an essential step is performed. The contrast adaptive histogram equalization (AHE) filter and Bayes wavelet transform (WT) are utilized to reduce noise, enhance brightness and contrast, and normalize the image. Figure 1 demonstrates the preprocessing steps. This process aims to remove noise from MRI images. The DB3 wavelet is used for decomposing the image, and the noise standard deviation is considered when establishing wavelet detail coefficient threshold. The type of wavelet applied is determined by `pywt.wavelist` function, with `bior6.8` selected as the wavelet choice. Soft thresholding is implemented to find the optimal match for the original image with additive noise. Contrast limited adaptive histogram equalization (CLAHE) is an advanced version of AHE designed to prevent contrast over amplification. CLAHE operates on small sections of the

image rather than the entire image, using a ClipLimit parameter to set contrast threshold. The initial value is set at 3, with the tile grid size determining the number of tiles per row and column set to 8×8. This approach applies a contrast filter by dividing the image into sections. The preprocessing stage concludes with cropping and normalizing MRI images. Cropping is a technique in computer imaging used to remove irrelevant areas and surroundings from images. Normalization is the process of reducing the intensity variation among pixel values, marking the final phase of the preprocessing stage.

2.2. Segmentation process

Image segmentation methods encompass threshold-based, edge-based, region-based, matching-based, clustering-based, fuzzy inference-based, and generalized principal component analysis techniques. Each method offers advantages and limitations. Clustering is a method for dividing a collection of objects into different groups, each known as a cluster. Members within each cluster exhibit high similarity in terms of features, but the degree of similarity compared to members of other clusters is minimal. While many clustering algorithms share foundational concepts, differences arise in how similarity or distance is measured and how labels are assigned to categories within each cluster. Key strategies include fuzzy clustering, density-based clustering, discriminative clustering, model-based clustering, and hierarchical clustering [17]. In our study, we have combined ImFCM clustering with Ws to enhance both the accuracy and efficiency of image analysis.

2.2.1. Improved fuzzy C-means clustering (the proposed method)

In fuzzy clustering, unlike traditional clustering where each sample is assigned exclusively to one cluster, a single sample can be associated with multiple clusters. The core principle behind fuzzy clustering is that each element can be assigned to different clusters with varying degrees of membership [18]. FCM is a widely recognized fuzzy clustering approach. Our objective is to optimize the following methodology [19] using the FCM algorithm:

$$J_m = \sum_{i=1}^c \sum_{k=1}^n u_{ik}^m d_{ik}^2 = \sum_{i=1}^c \sum_{k=1}^n u_{ik}^m \|x_k - v_i\|^2 \quad (1)$$

where m is a positive integer that is greater than one. Moreover, u_{ik} is the k_{th} data's level of membership in the i_{th} cluster, d_{ik} is the ratio of familiarity in the preceding n space, x_k indicates the k_{th} data, and v_i is the i_{th} cluster's center. In our study, we aim to develop an enhanced and robust fuzzy C-means (FCM) clustering technique, with modifications implemented in the following areas, as depicted in Figure 2.

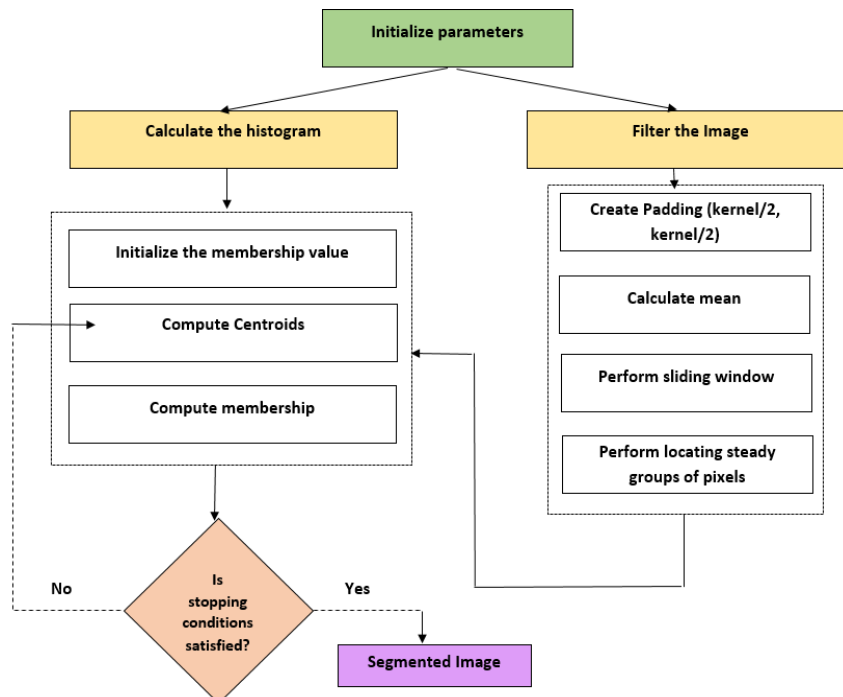


Figure 2. Improved fuzzy C-means clustering

First part (initial parameters setting): the parameter settings were carefully chosen as follows; we initially selected a cluster number of 4, as this count is considered optimal for segmenting MRI brain images into four distinct regions, effectively highlighting key tissues within the human brain. The fuzziness degree parameter was set to 2, providing increased flexibility in associating data with specific clusters, thereby achieving a balance between sensitivity and robustness. To ensure adequate convergence, a limit of 100 iterations was chosen, this decision being informed by observations from convergence experiments. A neighbor effect of 4 was selected to reflect the size of the sliding window used in image filtering, which facilitates the computation of local features and captures spatial relationships. An epsilon threshold of 0.05 was established for the convergence criteria, indicating a stringent convergence threshold due to its lower value. The kernel size was determined to be 3, to aid in capturing spatial information during the image filtering process.

Second part: the distance window has been utilized to filter the image. A sliding window technique is employed to traverse the entire image, aiming to identify stable groups. Initially, padding is created, equivalent to half of the kernel size, to ensure the inclusion of image borders during the sliding process. The image mean is calculated using this padding, and the `cv2.copyMakeBorder` function is employed to incorporate edges during sliding. Subsequently, a sliding window algorithm is defined, specifying the neighbor effect and window size as parameters, focusing on locating stable groups of pixels within clusters. The function for locating stable groups operates by identifying stable pixels through a Gaussian filter, where the filter's values are less than or equal to the square root of the nan mean for the power difference of Gaussian values and window size. The result of this phase is a filtered image, which will be further utilized in the third part to compute fuzziness.

Third part: the histogram of the image is determined using the CLAHE filter. It is to enhance image contrast and calculate the intensity distribution of the enhanced image. This phase is instrumental in determining the centroid of the cluster.

Fourth part: this segment encompasses several critical functions. It begins with the initialization of the membership function, which determines the degree to which the pixels of the image belong to each cluster. This is followed by the function for computing the centroids of the clusters, which involves the division of the numerator by the denominator. The numerator is the sum of the product of the degree of fuzziness, the histogram, and the intensity, each raised to the power of membership. Conversely, the denominator is the summation of the histogram values raised to the power of membership. The final step in this part is the computation of weights, a process reliant on the centroid computation function. This involves dividing the numerator by the denominator, where the numerator calculates the absolute differences between the intensity raised to a power and the computed cluster centroids. The denominator, on the other hand, sums the absolute differences, each raised to the power of the fuzziness degree. Algorithm 1 shows the detailed process. The block diagram in Figure 2 shows the process of utilizing the improved fuzzy C-means clustering.

Algorithm 1: ImFCM

```

Step 1: Initialize the following parameters:
- Number of bits. Number of clusters.
- Degree of fuzziness.
- Maximum iteration count.
- Epsilon threshold for convergence check.
Step 2: Image Filtering Procedure:
- Generate a padded image using a sliding window with dimensions (kernel_size/2,
  kernel_size/2).
- Compute the mean based on the padded mask.
- Pad the resulting mean image to create borders.
- Utilize a sliding window to account for neighbor effects and kernel size.
- Determine center coordinates using the spatial distance window with Minkowski
  distance:
  Des_win = ((abs (win_size_y - center_coordinate_y)) ** p + abs ((win_size_y -
  center_coordinate_y) ** p)) ** (1/p), where p = 2.
- Identify the stable group matrix using a Gaussian filter.
- Obtain the final filtered image using the formula:
  Final_image = sum (weighted_coefficients * old_window) / sum (weighted_coefficients)
- Perform CLAHE.
Step 3: Weight Initialization: Initialize a two-dimensional matrix based on the number of
clusters and gray levels to compute weights.
Step 4: Compute Cluster Centroids:
- Calculate the X and Y values as follows:
- X = sum (histogram * number of gray levels) * power (weight * number of fuzziness)
- Y = sum (histogram) * power (weight * number of fuzziness)
- Z = X / Y
Step 5: Weight Computation Method:
- Set power = -2 / number of fuzziness.
- Calculate the X value using the formula: X = (gray levels - centroid values) * power.

```

- Compute Y as: $Y = \text{sum}(\text{gray levels} - \text{centroid values}) * \text{power}$. Determine Z as: $Z = X / Y$.

Step 6: Check Convergence: Determine whether the absolute maximum value of (step 5 - step 2) is less than the epsilon threshold. If so, stop; otherwise, proceed to step 4.

2.2.2. Watershed segmentation

In Ws, an image is conceptualized in three dimensions, with the (x, y) coordinates correspond to the spatial axes and the intensity represented along the z-axis. This approach treats an image as if it were a topographical landscape, with the intensity of each pixel analogous to elevation levels. Consequently, each intensity level is associated with a distinct elevation plane on this landscape. Utilizing this topographical metaphor, points within the image are categorized into three segments: regional minima, catchment basins, and watershed lines. Catchment basin are areas were, hypothetical, a droplet of water would coverage towards a single regional minimum. Watershed lines, conversely, mark the boundaries where a droplet of water could potentially be drawn towards multiple regional minima, effectively delineating the division between distinct catchment basins [11].

Consider the M_1, M_2, \dots, M_R regional minima of an image $g(x, y)$. Let $T[n]$ represent an array of points beneath the horizontal axis with a value of n , where n ranges from the image's least to greatest intensity. This may be stated mathematically as follows:

$$T[n] = \{(s, t) | g(s, t) < n\} \quad (2)$$

$C_n(M_i)$ indicate a collection of regions in the catchment basin that are poured at plane n that are related with the region minimum M_i . This could possibly be used to compute it by:

$$C_n(M_i) = C(M_i)T[n] \quad (3)$$

$C(M_i)$ is the set of catchment basin points linked with the regional minimum M_i . The union of all flooded catchment basins at a certain stage n represented in $C[n]$:

$$C[n] = [C_n(M_i)] \quad (4)$$

Algorithm 2 introduces the steps of this technique. Figure 3 illustrate the watershed method in a block diagram.

Algorithm 2: Watershed segmentation

- Utilize OTSU's binarization filter to estimate the objects present in the image.
- Apply morphological opening to eliminate any white noise present in the image, and perform morphological closing to address small holes within the objects.
- Employ the dilate method to create a separation between the background and the image.
- Utilize distance transform and thresholding techniques to isolate the foreground from the background.
- Determine the unknown areas by subtracting the foreground from the background. These areas lacking clarity will be assigned zero values in the markers.
- Label the regions of the foreground using the connected components method as markers, and increment them by one to ensure all background regions are marked as ones.
- Employ the distance values obtained from step 5 and the markers from step 6 as input parameters for the watershed method to generate the final segmentation map.

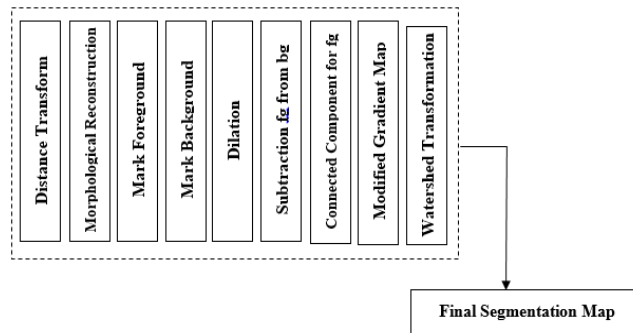


Figure 3. Watershed segmentation

2.3. Post-processing

Gamma correction is a technique used for data augmentation that entails adjusting the gamma value to modify the image intensity. Gamma represents a non-linear function that can be applied to either encode or decode the brightness or intensity of an image [20]. Gaussian noise, another form of distortion, is introduced into the image through random values drawn from a Gaussian distribution. Since noise encountered during image acquisition and preprocessing can escalate, applying Gaussian noise to a raw image may help the model become more resilient to variation in image quality [21]. Our study advocates for the use of these two methods as a post-processing measure for datasets that may suffer from loss in contrast and brightness, as well as to introduce a slight blurring effect to smooth transitions in pixel value and soften the image edges. The marker-controlled Ws technique is applied following the ImFCm twice with a marker value range of [10-90] to capture images highlighting internal brain features. This process is then repeated with a marker value range of [10-200] to obtain images showcasing external brain details. The culmination of this process involves combining all three images to produce the final enhanced image. Post-processing steps, including gamma correction and Gaussian blur, are subsequently performed to further refine the images, as depicted in Figure 4.

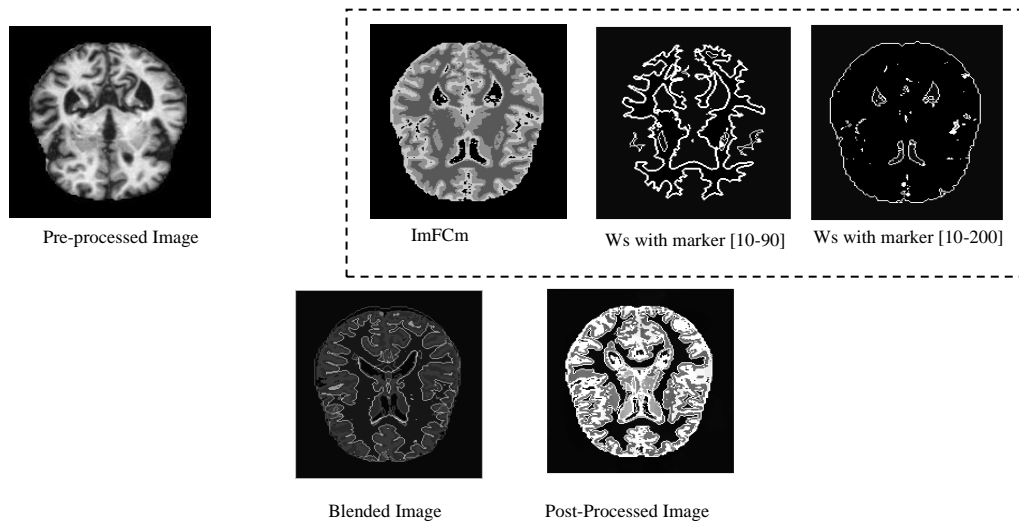


Figure 4. Segmentation stage

2.4. Classification

CNN, a cornerstone of the neural network framework, encompasses numerous layers within its architecture and has gained significant prominence in various image processing applications, notably in object recognition [22] and image classification, where it has yielded promising outcomes. Previous research indicates the feasibility of directly inputting images into a CNN network to extract features for image categorization. The architecture of a CNN comprises several fundamental components, including convolutional layers, SoftMax layers, pooling layers, non-linear activation functions such as the rectified linear unit (ReLU), and fully connected layers (FC) [23], [24]. CNNs operate based on the intensities of images, utilizing dimensions such as width, height, and depth to represent the input image intensities. The processing begins from the top left corner of the image and progresses to the right. As the filter moves from the top to the bottom of the input volume, it changes, with each left-to-right movement constituting a stride. The complexity of the stride is augmented by the number of steps it encompasses. ReLU serves as an efficient activation function by converting negative pixel values to zero [25]. Following the convolution process, the size of the hidden layer becomes significantly large, necessitating the use of a pooling or sub-sampling layer to reduce computational complexity. Pooling can be categorized into two types: maximum and average [26]. Within the context of pooling, let $y = y_{ij}$ represent the matrix.

$$ReLU(Y) = \max(0, Y) \quad (5)$$

As noticed in (6), max pooling is the process that selects the most significant component in y as the output

$$x = \max(y) \quad (6)$$

Our study analyzed MRI brain images from AD patients, organizing the dataset into four distinct categories: normal, mild, moderate, and very mild. Figure 5 illustrates a proposed CNN architectural model comprising 13 layers. This model includes four convolutional layers, with each pair of convolutions followed by a pooling layer and dropout layers to ensure regularization. The architecture concludes with a fully connected layer and a classifier layer. The original images, measuring 176×208 pixels, are resized to 200×200 pixels before being input into the CNN model. The filter size is varied across the CNN layers to effectively identify features. The batch size is set to 32, and the model undergoes training over 50 epochs. Upon completion of all epoch cycles, the CNN selects the model iteration with the highest performance metrics for classification purposes. The final classification is then applied to the test set to determine the accuracy rate.

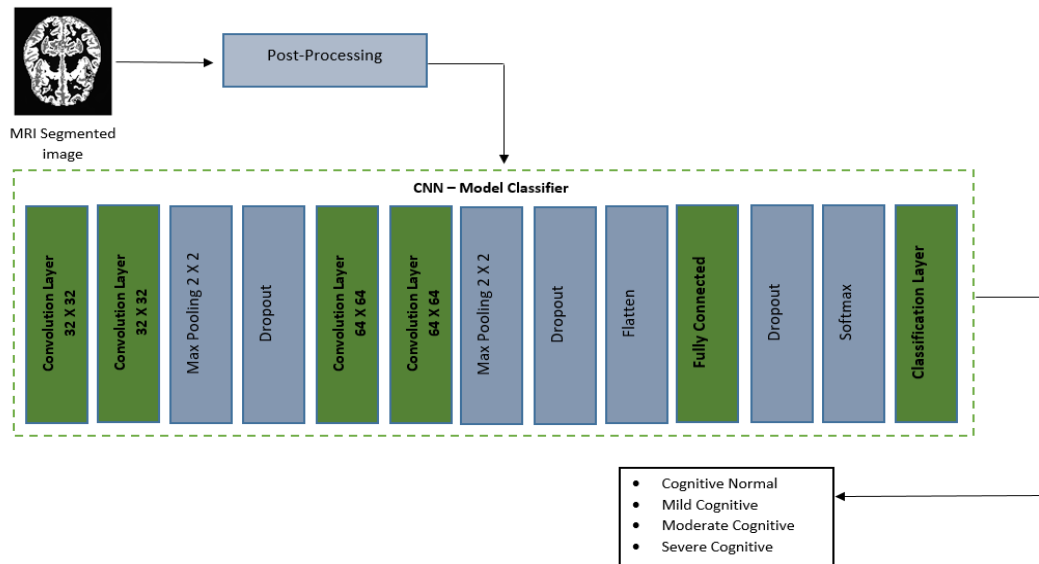


Figure 5. CNN model layers

Table 1 outlines the internal architecture of the CNN model, detailing the specific layers and configurations used within the model. Table 2 lists the hyperparameters applied during the model's training and optimization processes. For optimization, The Adam algorithm is utilized, with a learning rate of 0.001 set for the entire training phase.

Table 1. CNN model

Model layers	Image volume	Filters	Size of filter	Pooling win size	var.
conv2d (Conv2D)	(200, 200)	32	5x5	2x2	2432
conv2d_1 (Conv2D)	(200, 200)	32	5x5	2x2	25632
MaxPooling2D	(100, 100)	32		2x2	0
Dropout	(100, 100)	32			0
conv2d_2 (Conv2D)	(100, 100)	64	3x3		18496
conv2d_3 (Conv2D)	(100, 100)	64	3x3		36928
max_pooling2d_1	(50, 50)	64		2x2	0
dropout_1	(50, 50)	64			0
flatten (Flatten)	(None, 160000)				0
dense (Dense)	(None, 256)				40960256
dropout_2	(None, 256)				0
dense_1 (Dense)	(None, 4)				1028

Table 2. Values of hyper-parameters

Hyper-parameters	Value
Split data	3840 train, 1281 validate
Dropout	0.3, 0.3, 0.5
Batch size	32
Learning rate	0.001
Num. of epochs	50

3. RESULTS AND DISCUSSION

3.1. Experimental dataset

The MRI images utilized for this research were sourced from the ADNI database. A total of 6400 ADNI samples were selected for analysis after excluding certain samples with incorrect information. The dataset comprises 3140 normal samples, 896 early mild cognitive impairment samples, 64 moderate cognitive impairment samples, and 2240 severe cognitive impairment samples. These images are in JPEG format with a resolution of 176×208 pixels.

3.2. Evaluation metrics

3.2.1. Improved fuzzy C-means clustering

The evaluation criteria used to assess computational complexity focus on how efficiently our method performs in terms of computational resources used and the quality of results obtained. It involves evaluating the time and scalability of our method when applied to extensive datasets. Consideration is given to techniques or optimizations that could enhance the algorithm's efficiency without compromising accuracy. The used equation to compute the efficiency of our proposed method is depicted (7):

$$d = \sum_{i=1}^c \sum_{j=1}^n |U_{ij} - old_u_{ij}| \quad (7)$$

where d denotes the total absolute difference. c signifies the number of clusters. n represents the number of data points. U_{ij} reflects the membership value of data point j in cluster i during the current iteration. old_u_{ij} indicates the membership value of data point j in cluster i during the previous iteration. The equation calculates the sum of the absolute differences between corresponding elements of the current and prior membership matrices across all clusters and data points. This measurement can act as an indicator of convergence or change between successive iterations within an optimization algorithm, such as the fuzzy C-means clustering algorithm.

3.2.2. Convolutional neural network

The analysis of ML and DL recognition platforms, aimed at evaluating their capability to accurately diagnose AD, relies on several performance metrics, including accuracy (Acy), sensitivity (Sny)/recall, precision (Prn), and the F1 score. Each of these performance indicators offers different insights into the proposed model's effectiveness. The primary measure for evaluating the classification system is accuracy, which is calculated by dividing the number of correct predictions by the total number of predictions made. Mathematically, it can be expressed as (8):

$$Accuracy = \frac{T_p + T_N}{T_p + F_p + T_N + F_N} \quad (8)$$

where TP and TN are true positive and true negative respectively. FP, FN are false positive and false negative, respectively. Sensitivity and specificity are logically specified as (9):

$$Sensitivity = \frac{T_p}{T_p + F_N} \quad (9)$$

The sensitivity metric acts as an indicator of the effectiveness in detecting AD patients, reflecting the model's ability to correctly identify those who are truly affected by the disease. Precision measures the reliability of the diagnosis, representing the proportion of individuals identified by the system as having the disease who are indeed seriously impacted by it. This can be described as (10):

$$Precision = \frac{T_p}{T_p + F_p} \quad (10)$$

The F1 score of the simulation is described as the average of the sensitivity and accuracy.

$$F1 \text{ score} = 2 \times \left(\frac{Sny \times Prn}{Sny + Prn} \right) \quad (11)$$

3.3. Experimental results

3.3.1. Comparison results traditional fuzzy C-means and improved fuzzy C-means clustering

Upon completion of the ImFCm algorithm, convergence was achieved by the 35th iteration, thereby exceeding the preset maximum iteration threshold. The cost value experienced a significant reduction, descending from 385.01 to 0.049 as the iterations advanced. This decline signifies the algorithm's convergence

towards an optimal solution, highlighting the efficiency of our method in achieving results in a shorter timeframe. In comparison, the conventional FCM algorithm attained convergence at the 70th iteration, initiating with a cost value of 4907.9, and thus requiring more time relative to the proposed method. Figure 6 depicts the cost values for five different images alongside the duration taken by both the FCM and ImFCm algorithms.

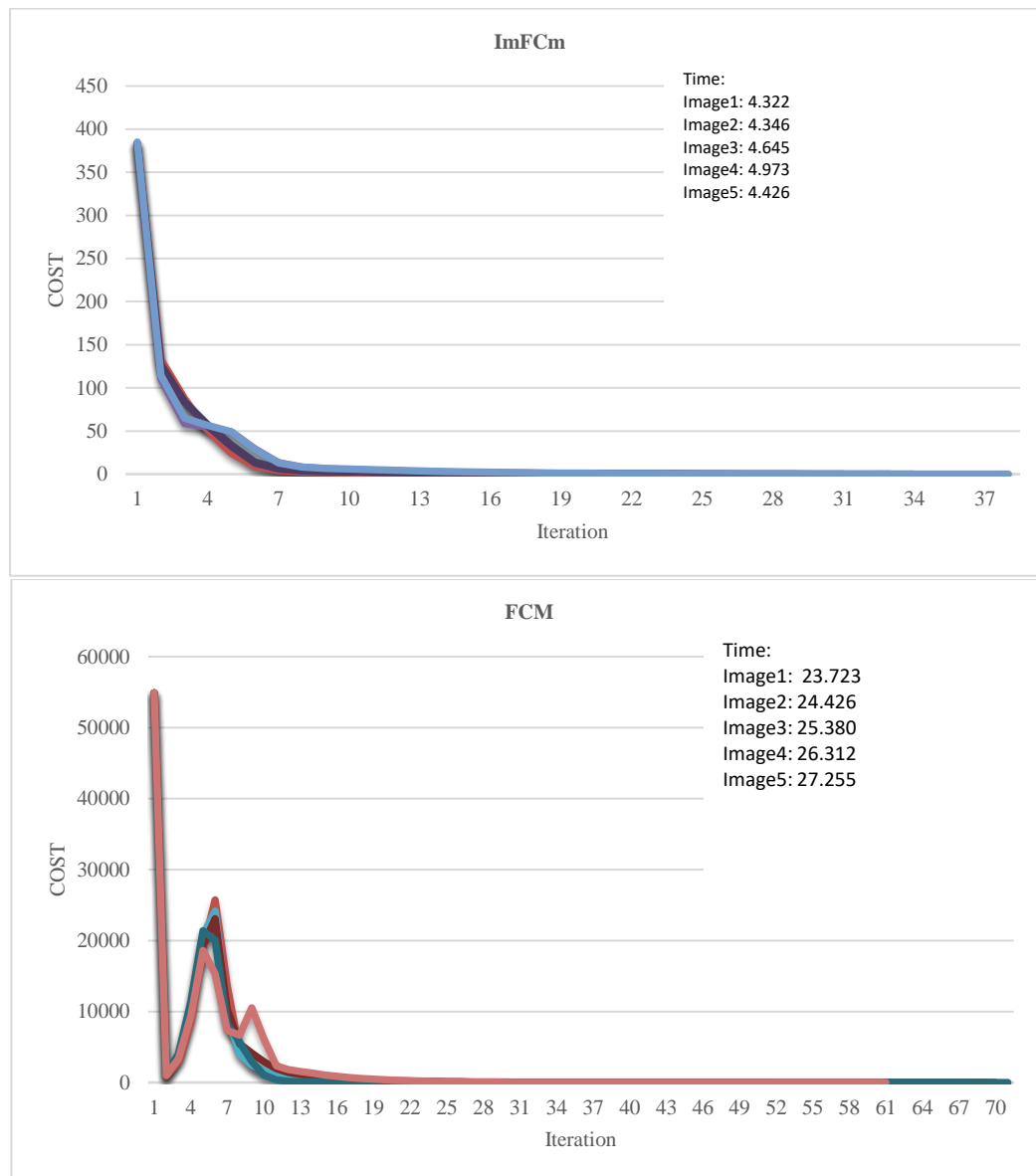


Figure 6. Cost and time for FCM and ImFCm

3.3.2. Convolutional neural network results with traditional fuzzy C-means

Traditional FCM clustering were employed for segmentation, which was then input into CNN for AD classification. Figure 7 illustrates the training and validation results from the segmented MRI brain dataset. The classification results demonstrated a test accuracy of 91% achieved over 50 epochs. One of the curves shows a red line representing training loss and a blue line for validation loss, while another curve illustrates a red line for validation accuracy and a blue line for accuracy. According to this technique, the figure indicates that both accuracy and validation accuracy converged after 10 epochs. The validation accuracy reached 0.88 and remained constant from epoch 14 through to epoch 50. By epoch 50, the loss decreased to 0.04, and the validation loss reached 0.6.

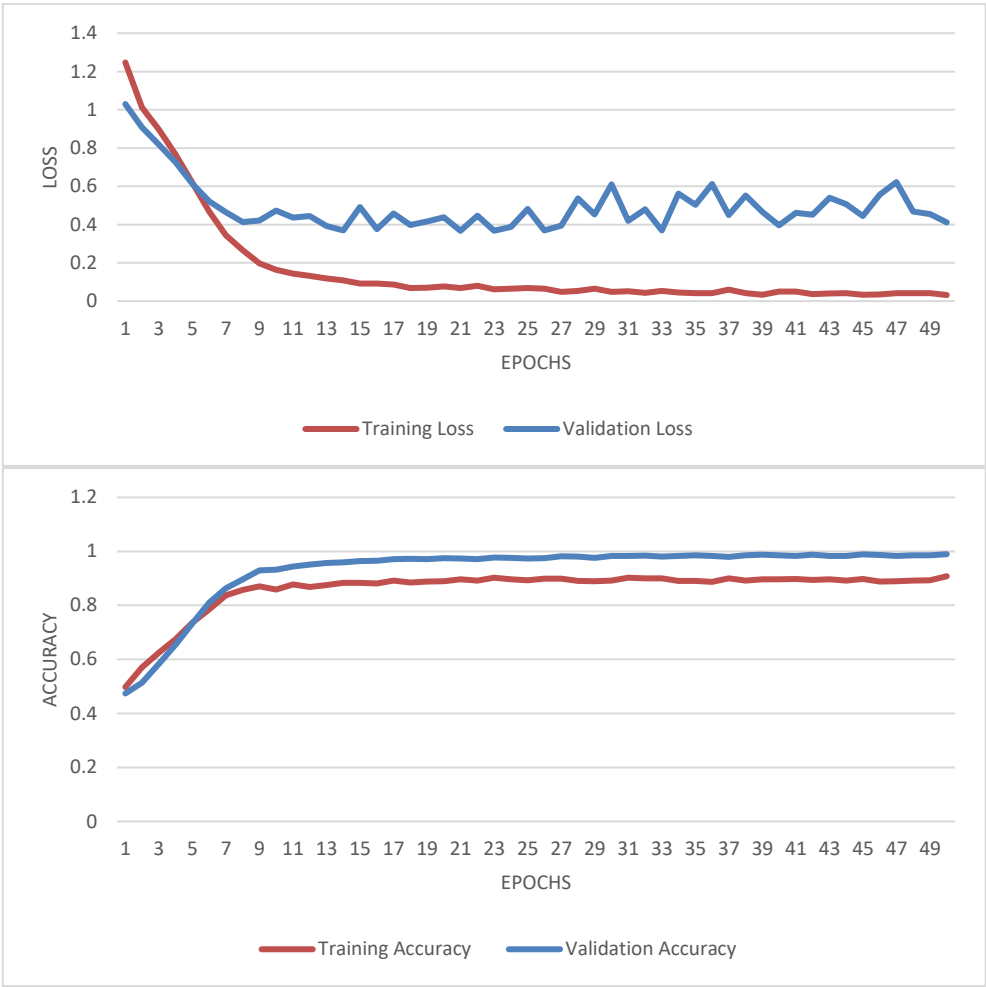


Figure 7. The accuracy and loss curves of classification for traditional FCM

Table 3 displays the classification report of the training model for each class using this segmentation technique. For the classes mild, normal, moderate, and very mild, the precisions were 91%, 100%, 91%, and 90%, respectively. The recall rates for these classes were 79%, 89%, 95%, and 90% in that order. The F1-scores for the classes are 85%, 94%, 93%, and 90%, respectively.

Table 3. Classification Report of Traditional FCM			
Class Name	Precision	Recall	F1-Score
Mild	0.91	0.79	0.85
Normal	1.00	0.89	0.94
Moderate	0.91	0.95	0.93
Very mild	0.90	0.90	0.90
Accuracy 91% for predictions			

3.3.3. Convolutional neural network results with improved fuzzy C-means clustering

The outcomes of the proposed classification process, as applied to both the training and validation sets, are illustrated through accuracy and loss curves in Figure 8. The figure reveals that convergence of the training approach's accuracy and loss was observed after 10 iterations, indicating high training and testing accuracy. The training accuracy achieved is in the vicinity of 99%, accompanied by a loss of approximately 3%, whereas the validation accuracy approaches 98%, with a loss near 6%. Analysis of the figures demonstrates that the discrepancy between training accuracy and validation accuracy, as well as between training loss and validation loss, is minimal. Consequently, 50 epochs have been deemed suitable for the training and verification of our model. Figure 8 further indicates that after the initial 10 epochs, the accuracy for both training and

validation has stabilized. Based on these results, it can be concluded that the method we proposed has enhanced the model's efficiency, enabling it to be trained and validated within fewer epochs.

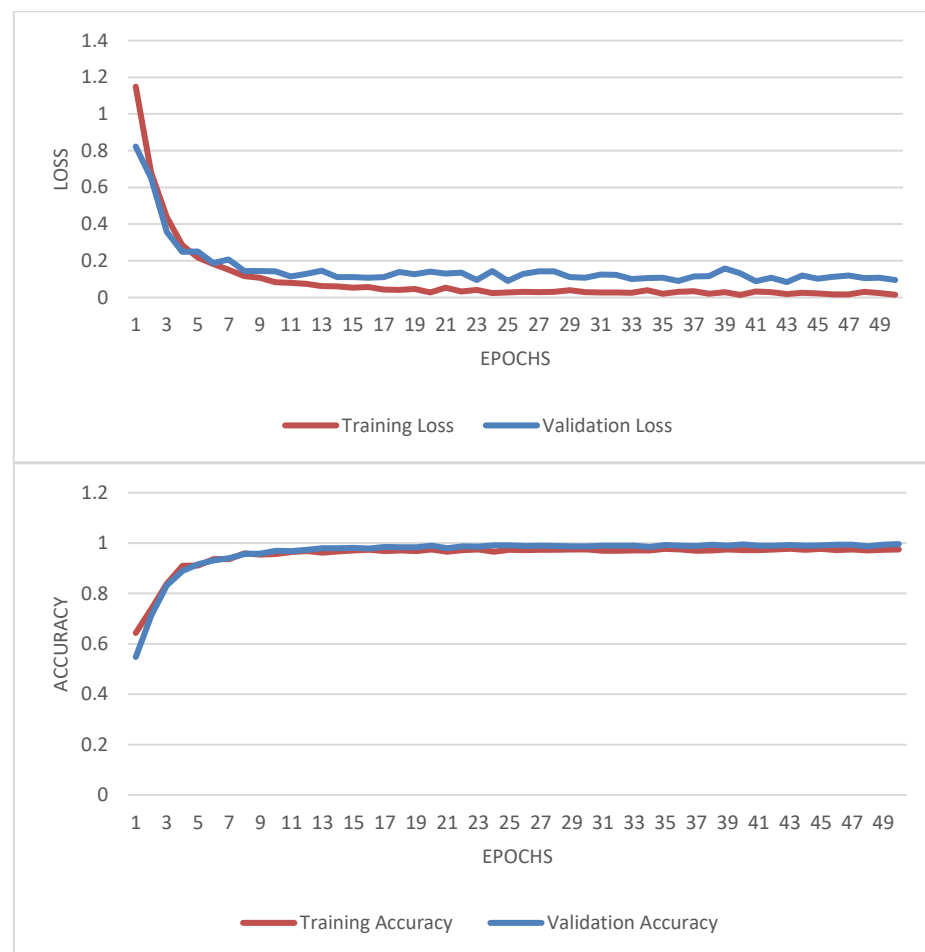


Figure 8. The accuracy and loss curves of the proposed classification results

By integrating two powerful segmentation techniques, the updated model reveals more detailed features. The attributes derived from these hybrid methods are varied; by combining them, the features become more robust, enhancing the classification phase. Table 4 displays the classification report of the training model for each class. For the classes mild, normal, moderate, and very mild, the precisions were 97%, 100%, 99%, and 97%, respectively. The recall rates for these classes were 99%, 100%, 98%, and 99%, in that order. The F1-scores for the classes are 98%, 100%, 98%, and 98%, respectively. The outcomes of the adapted model used in this study generally demonstrate exceptional performance, indicating that employing advanced MRI segmentation techniques to enhance AD diagnostic classification performance is beneficial. After comprehensive training, the system undergoes evaluation using a testing set, which consists of images that were not exposed to the system during the training phase. Employing our recommended segmentation technique, the CNN model achieves an accuracy of 98.98% and demonstrates efficient performance on MRI images.

Table 4. Classification report of the proposed method

Class name	Precision	Recall	F1-Score
Mild	0.97	0.99	0.98
Normal	1.00	1.00	1.00
Moderate	0.99	0.98	0.98
Very mild	0.97	0.99	0.98
Accuracy 98.20% for predictions			

3.4. Comparative examination from diverse researches models

Our proposed methodology distinguishes itself through a comparative analysis with existing research efforts aimed at early AD detection, utilizing a detailed four-class classification framework, as detailed in Table 5. The suggested ImFCm-Ws-CNN model exhibits notable advancements in accuracy, precision, and F1-score metrics. It achieves an impressive 96.25% accuracy, 98.0% precision, and a 97% F1 score, surpassing the performance of previous studies. This comparative assessment underscores the advantages of incorporating ImFCm-Ws techniques into CNN models, highlighting enhanced diagnostic capabilities without sacrificing performance metrics.

Table 5. A summary of new studies implementing techniques using DL

Ref.	Image	Dataset	Extracted Features	Classifier	Acc	precision	Recall	F1	Others
[27]	T1-MRI	MIRIAD	---	CNN	89.0	89.0	89.0	89.0	AD Vs Non
[28]	MRI	OASIS	---	HT-MGWRO	93.16	90.74	94.23	92.45	AD Vs Non
[29]	MRI+EEG	ADNI+Rowan Univ	Texture properties of an image	Hybrid CNN+DBN	92.50	---	90.89	---	AD Vs Non
[30]	MRI	ADNI	FreeSurfer	DNN	85.19	76.93	72.73	74.77	Multiclass
[12]	SMRI (T1)	ADNI	3D Patches	Hybrid multi-task deep CNN and DenseNet+softmax	88.90	---	88.60	---	AD Vs Non
[31]	MRI	ADNI	Bag of Features (BoF)	SVM	93	---	---	---	Multiclass
[32]	MRI	OASIS	Statistical measures of the mean and standard deviation	Hybrid AlexNet+SVM	94.0	93.0	97.0	---	Multiclass
[11]	MRI, PET, Cognitive scores, Neuropathology, assessment	ADNI	Local and longitudinal features	Stacked CNN-BiLSTM	92.62	---	98.42	---	AD progression
Proposed	MRI	ADNI	ImFCm-Ws	CNN	98.20	98	98	98	Multiclass

4. CONCLUSION

This study introduces a novel methodology for the precise identification of AD progression through the integration of feature extraction using the ImFCM-Ws technique with an optimized CNN architecture. Utilizing the standardized ADNI dataset, our model effectively categorizes the different stages of AD. The evaluation revealed that the CNN model, enhanced with ImFCM-Ws features, outperformed existing methods, achieving an exceptional accuracy of 98.20%. Through meticulous feature extraction, our approach accurately identifies brain regions associated with Alzheimer's pathology, providing invaluable assistance to healthcare professionals in evaluating the disease's severity based on levels of dementia. By allowing the data to inform our analysis, our findings underscore the significance of our methodology in improving the detection and diagnosis of AD. On the other hand, several limitations must be introduced despite the results and promising contributions of our study. One of these limitations, our approach relies on the ADNI dataset, which, although comprehensive, may not include all data sources in AD. This limitation could introduce bias if inaccuracies have occurred in generalizing our model to specific populations or cases with specific characteristics. To prevent this limitation, we suggest for future to add multimodal data sources such as neuroimaging scans, genetic information, and clinical assessments that could refine our model to capture additional information to detect this disease.

5. FUTURE WORK

Our study employs a synergistic approach, combining ImFCm with Ws for effective feature extraction, and leveraging CNN for classification. While our findings illuminate the effectiveness of this methodology in detecting AD, several areas warrant further investigation. Future research could focus on optimizing the parameters and algorithms of ImFCm and Ws to enhance the accuracy and efficiency of feature

extraction. Additionally, the exploration of innovative fusion techniques for integrating multimodal neuroimaging data may significantly enhance the diagnostic accuracy and robustness of the classification model. Moreover, the application of advanced ML and DL architectures beyond CNN, such as recurrent neural networks (RNNs) or graph neural networks (GNNs), could provide novel perspectives on AD diagnosis and progression monitoring. These prospective research avenues aim to propel forward the domain of neuroimaging-based AD detection, contributing towards the creation of more precise and dependable diagnostic tools.




REFERENCES

- [1] Alzheimer's Dementia, "2020 Alzheimer's disease facts and figures," *The Journal of the Alzheimer's Association*, Mar. 2020, pp. 391–460, doi: 10.1002/alz.12068.
- [2] G. Liu, Q. Lin, N. N. Xiong, and X. Wang, "Unsupervised denoising feature learning for classification of corrupted images," *Big Data Research*, vol. 27, Feb. 2022, doi: 10.1016/j.bdr.2021.100305.
- [3] M. Liu, M. Zhou, T. Zhang, and N. Xiong, "Semi-supervised learning quantization algorithm with deep features for motor imagery EEG Recognition in smart healthcare application," *Applied Soft Computing*, vol. 89, Apr. 2020, doi: 10.1016/j.asoc.2020.106071.
- [4] D. Li *et al.*, "CARM: Confidence-aware recommender model via review representation learning and historical rating behavior in the online platforms," *Neurocomputing*, vol. 455, pp. 283–296, Sep. 2021, doi: 10.1016/j.neucom.2021.03.122.
- [5] C. Wu, C. Luo, N. Xiong, W. Zhang, and T.-H. Kim, "A greedy deep learning method for medical disease analysis," *IEEE Access*, vol. 6, pp. 20021–20030, 2018, doi: 10.1109/ACCESS.2018.2823979.
- [6] G. Litjens *et al.*, "A survey on deep learning in medical image analysis," *Medical Image Analysis*, vol. 42, pp. 60–88, Dec. 2017, doi: 10.1016/j.media.2017.07.005.
- [7] L. Sun, W. Shao, M. Wang, D. Zhang, and M. Liu, "High order feature learning for multi-atlas based label fusion: application to brain segmentation with MRI," *IEEE Transactions on Image Processing*, vol. 29, pp. 2702–2713, 2020, doi: 10.1109/TIP.2019.2952079.
- [8] E. H. Ali, S. Sadek, and Z. F. Makki, "A review of AI techniques using MRI brain images for Alzheimer's disease detection," in *2023 Fifth International Conference on Advances in Computational Tools for Engineering Applications (ACTEA)*, Jul. 2023, pp. 76–82, doi: 10.1109/ACTEA58025.2023.10194002.
- [9] G. Currie, K. E. Hawk, E. Rohren, A. Vial, and R. Klein, "Machine learning and deep learning in medical imaging: intelligent imaging," *Journal of Medical Imaging and Radiation Sciences*, vol. 50, no. 4, pp. 477–487, Dec. 2019, doi: 10.1016/j.jmir.2019.09.005.
- [10] I. Cherian, M. Alate, A. B. Desai, M. R. Prajna, and D. Rawat, "Early detection of alzheimer's disease using fuzzy C-means clustering and genetic algorithm-based feature selection from PET scan," *International Journal of Intelligent Systems and Applications in Engineering*, vol. 12, no. 3s, pp. 452–463, 2023.
- [11] S. E.-Sappagh, T. Abuhmed, S. M. Riazul Islam, and K. S. Kwak, "Multimodal multitask deep learning model for Alzheimer's disease progression detection based on time series data," *Neurocomputing*, vol. 412, pp. 197–215, Oct. 2020, doi: 10.1016/j.neucom.2020.05.087.
- [12] M. Liu *et al.*, "A multi-model deep convolutional neural network for automatic hippocampus segmentation and classification in Alzheimer's disease," *NeuroImage*, vol. 208, Mar. 2020, doi: 10.1016/j.neuroimage.2019.116459.
- [13] L. Nanni, S. Brahnam, C. Salvatore, and I. Castiglioni, "Texture descriptors and voxels for the early diagnosis of Alzheimer's disease," *Artificial Intelligence in Medicine*, vol. 97, pp. 19–26, Jun. 2019, doi: 10.1016/j.artmed.2019.05.003.
- [14] C. Geetha and D. Pugazhenthii, "Classification of alzheimer's disease subjects from MRI using fuzzy neural network with feature extraction using discrete wavelet transform," *Biomedical Research*, pp. S14–S21, 2018, doi: 10.4066/biomedicalresearch.29-16-2319.
- [15] B.-K. Choi *et al.*, "Convolutional neural network-based MR image analysis for Alzheimer's disease classification," *Current Medical Imaging Formerly Current Medical Imaging Reviews*, vol. 16, no. 1, pp. 27–35, Jan. 2020, doi: 10.2174/1573405615666191021123854.
- [16] X. Bi, X. Zhao, H. Huang, D. Chen, and Y. Ma, "Functional brain network classification for Alzheimer's disease detection with deep features and extreme learning machine," *Cognitive Computation*, vol. 12, no. 3, pp. 513–527, May 2020, doi: 10.1007/s12559-019-09688-2.
- [17] T. Singh, N. Saxena, M. Khurana, D. Singh, M. Abdalla, and H. Alshazly, "Data clustering using moth-flame optimization algorithm," *Sensors*, vol. 21, no. 12, Jun. 2021, doi: 10.3390/s21124086.
- [18] E. H. Ruspini, J. C. Bezdek, and J. M. Keller, "Fuzzy clustering: A historical perspective," *IEEE Computational Intelligence Magazine*, vol. 14, no. 1, pp. 45–55, Feb. 2019, doi: 10.1109/MCI.2018.2881643.
- [19] R. Xu and D. WunschII, "Survey of clustering algorithms," *IEEE Transactions on Neural Networks*, vol. 16, no. 3, pp. 645–678, May 2005, doi: 10.1109/TNN.2005.845141.
- [20] A. Zhong *et al.*, "Deep metric learning-based image retrieval system for chest radiograph and its clinical applications in COVID-19," *Medical Image Analysis*, vol. 70, 2021, doi: 10.1016/j.media.2021.101993.
- [21] I. Sirazitdinov, M. Kholiavchenko, R. Kuleev, and B. Ibragimov, "Data augmentation for chest pathologies classification," in *2019 IEEE 16th International Symposium on Biomedical Imaging (ISBI 2019)*, Apr. 2019, pp. 1216–1219, doi: 10.1109/ISBI.2019.8759573.
- [22] L. J. Belaid and W. Mourou, "Image segmentation: A watershed transformation algorithm," *Image Analysis & Stereology*, vol. 28, no. 2, pp. 93–102, May 2011, doi: 10.5566/ias.v28.p93-102.
- [23] N. A. Mohammed, M. H. Abed, and A. T. A. -Salih, "Convolutional neural network for color images classification," *Bulletin of Electrical Engineering and Informatics*, vol. 11, no. 3, pp. 1343–1349, Jun. 2022, doi: 10.11591/eei.v11i3.3730.
- [24] K. O'Shea and R. Nash, "An introduction to convolutional neural networks," *arXiv-Computer Science*, pp. 1–11, Nov. 2015.
- [25] R. Poojary, R. Raina, and A. Kumar Mondal, "Effect of data-augmentation on fine-tuned CNN model performance," *IAES International Journal of Artificial Intelligence (IJ-AI)*, vol. 10, no. 1, pp. 84–92, Mar. 2021, doi: 10.11591/ijai.v10.i1.pp84-92.
- [26] F. Fachrudin, S. Saparudin, E. Rasywir, and Y. Pratama, "Network and layer experiment using convolutional neural network for content based image retrieval work," *TELKOMNIKA (Telecommunication Computing Electronics and Control)*, vol. 20, no. 1, pp. 118–128, Feb. 2022, doi: 10.12928/telkomnika.v20i1.19759.
- [27] K. D. Silva and H. Kunz, "Prediction of Alzheimer's disease from magnetic resonance imaging using a convolutional neural




- network,” *Intelligence-Based Medicine*, vol. 7, 2023, doi: 10.1016/j.ibmed.2023.100091.
- [28] N. Bharanidharan and R. Harikumar, “Modified grey wolf randomized optimization in dementia classification using MRI images,” *IETE Journal of Research*, vol. 68, no. 4, pp. 2531–2540, Jul. 2022, doi: 10.1080/03772063.2020.1715852.
- [29] A. Shikalgar and S. Sonavane, “Hybrid deep learning approach for classifying Alzheimer disease based on multimodal data,” in *Computing in Engineering and Technology*, 2020, pp. 511–520, doi: 10.1007/978-981-32-9515-5_49.
- [30] R. Prajapati, U. Khatri, and G. R. Kwon, “An efficient deep neural network binary classifier for Alzheimer’s disease classification,” in *2021 International Conference on Artificial Intelligence in Information and Communication (ICAIIIC)*, Apr. 2021, pp. 231–234, doi: 10.1109/ICAIIIC51459.2021.9415212.
- [31] H. Guo and Y. Zhang, “Resting state fMRI and improved deep learning algorithm for earlier detection of Alzheimer’s disease,” *IEEE Access*, vol. 8, pp. 115383–115392, 2020, doi: 10.1109/ACCESS.2020.3003424.
- [32] B. A. Mohammed *et al.*, “Multimethod analysis of medical records and MRI images for early diagnosis of dementia and Alzheimer’s disease based on deep learning and hybrid methods,” *Electronics*, vol. 10, no. 22, Nov. 2021, doi: 10.3390/electronics10222860.

BIOGRAPHIES OF AUTHORS






Esraa H. Ali    holds both an M.Sc. and B.Sc. degree from Al-Nahrain University, Iraq, which were attained in 2009. Presently, she serves as an assistant lecturer at the Department of Computer Science within the College of Science at Al-Nahrain University, located in Baghdad, Iraq. Her expertise lies in the field of image processing. Her research interests encompass image processing, machine learning, and audio cryptography. To date, she has authored approximately 7 papers featured in international journals and conferences. She can be contacted at email: esraa.ali@ul.edu.iq or esraa.hussien@nahrainuniv.edu.iq.



Sawsan Sadek    holds a Ph.D. in electronics from the University of Science and Technology in Lille, France in 1996 and a Bachelor's degree of Physics from the Lebanese University in 1990. Currently she is a Professor at the Lebanese University, Faculty of Technology in Saïda, Lebanon, Department of Communications and Information Networks. She headed the department for 5 years from 2009 to 2014. She organized the thirteenth edition of the IEEE MMS2013, and launched the first global conference on sensor networks and smart technologies in Beirut IEEE SENSET2017 and issued a special edition of the scientific journal ALOG Springer. She has many research papers in international scientific journals and conferences and supervised many doctoral theses in cooperation with French universities. She can be contacted at email: sawsansadek@yahoo.fr or dsadek@ul.edu.lb.



Dr. Zaid F. Makki    holds Ph.D. Degree in Computer Information Systems (CIS) from the Lebanese University in 2019. He also received his master's degree of Computer Information Systems (CIS) Middle East University, Jordan, in 2012. He also holds a master's degree in Educational Administration and Leadership, Middle East University, Jordan, in 2015. He is currently a Governance Advisor in the General Secretariat of the council of Ministers and he is the Head of the digital transformation team Office of the Prime Minister Scientific and Technological Advisor, he also occupies on behalf of National Security Advisory Director General of the National Spatial Data Center of the Iraqi government. He can be contacted at email: zaidfj@coeng.uobaghdad.edu.iq.